arXiv:1609.04993v1 [physics.atom-ph] 16 Sep 2016

SSPALS for atomic physics with positronium

Adam Deller

Department of Physics and Astronomy, University College London, Gower Street, London, WC1E 6BT, UK

E-mail: a.deller@ucl.ac.uk

Abstract. Single-shot positron annihilation lifetime spectroscopy (SSPALS) has proven an extremely useful tool for atomic physics experiments with positronium (Ps). Using a Monte-Carlo simulation, I examine methods employed to analyze lifetime spectra and explore the advantages and limitations these have in laser spectroscopy experiments, such as resonance-enhance multiphoton ionization (REMPI) or the production of Rydberg Ps.

1. Introduction

Positronium (Ps) [1, 2] is the bound state of an electron and a positron. In vacuum, the two components will ultimately annihilate with each other. The mean lifetime against self-annihilation is 125 ps for the $n = 1$ singlet spin state ($S = 0$, para-Ps) [3], or 142 ns for the $n = 1$ triplet spin states ($S = 1$, ortho-Ps) [4]. Annihilation of p-Ps usually results in two 511 keV gamma-ray photons, whereas o-Ps predominately decays into three with a combined energy of 1.022 MeV [5]. A scintillator coupled to a photomultiplier tube (PMT) can be used to efficiently detect gamma rays with sub-ns timing resolution [6]. This facilitates precision positron annihilation lifetime spectroscopy (PALS) [7, 8] – a simple but invaluable tool for studying Ps.

The atomic structure of Ps [9] can be described at the principal level by the Bohr model of hydrogen rescaled by 1/2. Optical excitation from the ground state can be achieved using a pulsed laser ($\sim$ 5 ns) synchronized to a time-bunched Ps source ($\lesssim$ 10 ns) [10–15]. Conventionally, to measure a PALS spectrum each annihilation event must be distinguishable, which is not compatible with pulsed Ps sources. In this case, single-shot positron annihilation lifetime spectroscopy (SSPALS) [16] can be used. Here, the output of a fast gamma-ray detector constitutes the lifetime spectrum. This is a valid approximation if the Ps formation time and the decay time of the detector are both sufficiently short. With a scintillation decay time of $\sim$ 10 ns, $PbWO_4$ is a suitable material for resolving o-Ps decay ($\tau = 142$ ns). A faster material, such as the Cerenkov radiator PbF_2, can provide better timing resolution [17]. For some applications, a slower material that has a higher light output, such as LYSO, might be a better choice [18].

Pulsed Ps sources, with time widths of a few ns, can be obtained by implanting time-focused positron beams [19, 20] into Ps-converter materials, such as mesoporous SiO_2 [21, 22]. The interconnected mesoporous network provides a path to vacuum along which Ps atoms may cool via inelastic collisions [12, 23]. The overall efficiency for emission of o-Ps from mesoporous silica is typically $\epsilon \approx 0.3$ /e$^+$. Other materials are known to be more efficient Ps-converters [e.g., 24], however, mesoporous silica is often chosen for laser spectroscopy experiments because it performs well at room temperature and the conversion efficiency is generally stable [25]. Moreover, most Ps atoms emitted from this material possess low kinetic energy ($\sim$ 40 meV, roughly equivalent

to 500 K). Without a hadron-laden nucleus to weigh it down, a Ps atom will usually move at high speed ($|\vec{v}| \approx 8.4 \times 10^4$ ms^{-1} for $E = 40$ meV). For a 500 K distribution the Doppler width of the $1S \rightarrow 2P$ transition is around 1 THz, and laser bandwidths $\gtrsim$ 100 GHz are required to achieve significant spectral overlap [11–13, 26]. Having a narrow velocity distribution is, therefore, important for driving a single-photon transition. Alternatively, two-photon Doppler-free excitation schemes can be pursued [10, 27].

There are unique challenges to performing atomic physics experiments with positronium that arise from its low mass and propensity to self-annihilate. On the other hand, annihilation radiation can be taken advantage of, e.g., for measuring lifetime spectra. In this article, I employ Monte-Carlo techniques to simulate Ps distributions and their lifetime spectra, with a view to exploring the application of SSPALS to laser spectroscopy experiments with Ps.

2. Single-shot positron annihilation lifetime spectra

The lifetime spectrum observed when a pulsed positron beam impacts a Ps-converter will, in general, contain two main features: (i) a prompt peak associated with the rapid annihilation of e^+ and p-Ps; (ii) delayed events that reflect the exponential decay of o-Ps.

An SSPALS spectrum can be modelled using a Gaussian distribution for the positron implantation time (width of σ), convolved with the ϵ-weighted decay of o-Ps ($\tau = 142$ ns); I use the approximation that unconverted positrons and p-Ps annihilate immediately, and that the product of the likelihood of detecting an event and its amplitude is equal for 3γ and 2γ decay. This function can then be convolved with a model for the detector response (rise time of zero and decay time of κ). Altogether, this gives

$$V(t) = V_0 \exp\left[-t\left(\frac{1}{\kappa}+\frac{1}{\tau}\right)\right]\left(\epsilon \exp\left[\frac{\sigma^2}{2\tau^2}+\frac{t}{\kappa}\right]\left(1+\operatorname{erf}\left[\frac{t\tau-\sigma^2}{\sqrt{2}\sigma\tau}\right]\right)-\left(1+\frac{\tau}{\kappa}(\epsilon-1)\right)\exp\left[\frac{\sigma^2}{2\kappa^2}+\frac{t}{\tau}\right]\left(1+\operatorname{erf}\left[\frac{t\kappa-\sigma^2}{\sqrt{2}\sigma\kappa}\right]\right)\right), \quad (1)$$

where V_0 is an arbitrary scaling factor; exp and erf denote the exponential and the error function, respectively. This equation is plotted in Fig. 1 for typical positron pulse and Ps-converter parameters and a detector response appropriate to $PbWO_4$ ($\kappa = 10$ ns).

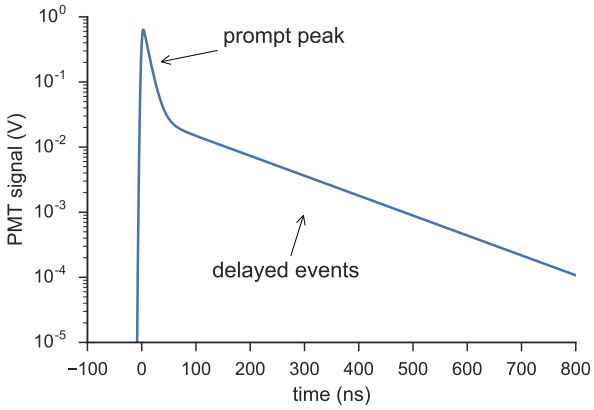

Figure 1. An SSPALS spectra modelled using Eq. 1 ($\epsilon = 0.3$, $\kappa = 10$ ns, and $\sigma = 2$ ns).

In principle, Eq. 1 can be fitted to a measured spectrum to deconvolve its components. In practice, however, it is normally sufficient to quantify the delayed fraction. This metric can be

used to estimate of the Ps conversion efficiency or to observe, e.g., laser-induced changes in the spectra. The delayed fraction is here defined as

$$f_d = \frac{\int_B^C V(t)\,dt}{\int_A^C V(t)\,dt}, \tag{2}$$

where the time interval $A \to B$ encompasses the prompt peak and $B \to C$ contains the delayed events. Typical choices for these parameters are $A = -10$ ns, $B = 30$ ns, and $C = 800$ ns, where $t = 0$ is given by the positron implantation time. In general, the exact values of A and C are not important, so long as the bulk of the spectra is captured. The choice of B, however, will depend on the process being measured.

In Ref. [28] the relationship between the Ps conversion efficiency and the measured delayed fraction was examined using an exponential response model for the prompt and delayed components of SSPALS spectra. In the present work, I calculate f_d for spectra modelled using Eq. 1 with $\kappa = 10$ ns and $\sigma = 2$ ns. Fig. 2a illustrates that for $B = 30$ ns the delayed fraction tracks the Ps conversion efficiency fairly accurately, especially in the region close to $\epsilon = 0.3$. Similarly, Fig. 2b shows how the difference between the delayed fraction and the conversion efficiency varies with the choice of B, indicating that the broadest range of agreement is found in the region of $B = 20$ to 40 ns. Note, however, that this will depend on the time width of the positron pulse and the time response of the detector [e.g., 17, 18].

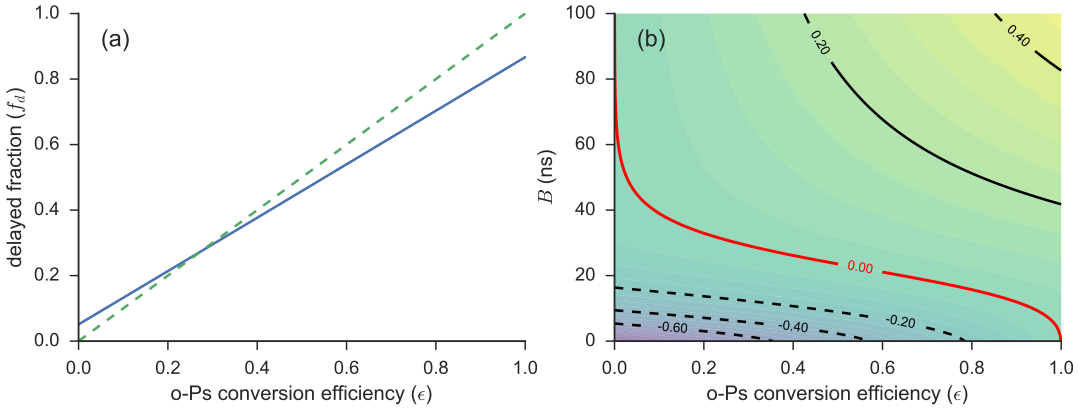

Figure 2. (a) The delayed fraction measured for SSPALS spectra modelled using Eq. 1 ($\tau = 142$ ns, $\kappa = 10$ ns, and $\sigma = 2$ ns). The integration bound B is 30 ns. The dashed line marks $y = x$. (b) Contour plot of the difference between the Ps conversion efficiency and the delayed fraction ($\epsilon - f_d$) as a function of ϵ and B. Negative contours are dashed.

For many applications the absolute value of the o-Ps fraction is not important – what matters is how it changes. As demonstrated in this section, the delayed fraction provides a very simple means of quantifying a spectrum which is sensitive to, and varies almost linearly with, the number of o-Ps decay events contributing to it. Changes to the delayed fraction, f_d, are normally measured using the parameter

$$S_\gamma = \frac{f_{bk} - f_d}{f_{bk}}, \tag{3}$$

where f_{bk} is a background measurement of the delayed fraction (e.g., no laser).

3. Laser spectroscopy

3.1. Experimental methods

A setup for creating Ps atoms and interrogating them with lasers is shown in Fig. 3. Here, a magnetic field guides a positron pulse into a Ps-converter material (e.g., mesoporous SiO_2) mounted to a target electrode. The voltage applied to the electrode is used to tune the positron implantation energy (typically, 1 - 5 keV). Some fraction of the positrons will form Ps that is emitted to vacuum, where they can be intersected by one or more laser pulses. A nearby gamma-ray detector records the SSPALS spectrum. In some cases, an additional electrode or a grid, offset and parallel to the target, is used to control the electric field in the laser-interaction region [14, 29, 30].

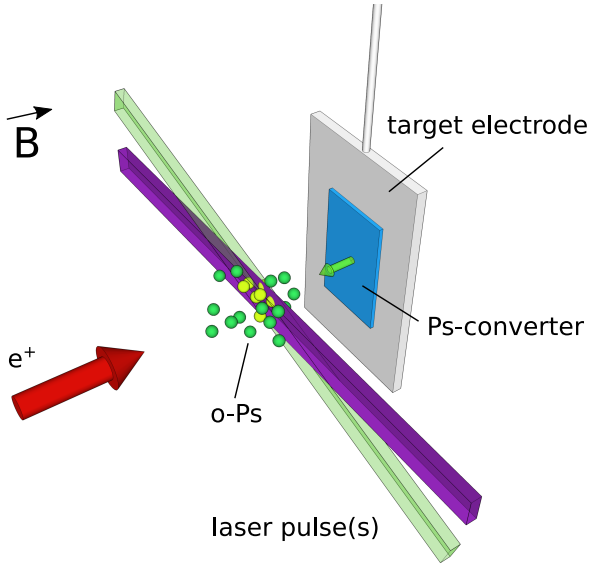

Figure 3. Schematic of a simple Ps-formation and laser-interaction experimental configuration. A time-focused positron bunch is implanted into a Ps-converter material and lasers intersect the emitted Ps atoms.

3.2. Reducing the lifetime of positronium

Quenching and ionization can reduce the mean lifetime of a Ps ensemble and thereby affect its lifetime spectrum. These processes can be resonantly induced for spectroscopy using lasers. For example:

(i) Magnetic quenching [31], where an applied magnetic field mixes singlet and triplet states. The $2P$ levels are more readily mixed than the ground state and can be populated using a $\lambda = 243.0$ nm (UV) laser [11, 13, 32]. Mixing can be enhanced (or suppressed) using an electric field [29, 30]. Although the annihilation lifetimes of the $2P$ states are very long [33, 34] the fluorescence lifetime is just 3.2 ns. Rapid annihilation follows decay from an excited mixed state to the short-lived singlet ground state (p-Ps).

(ii) Photoionization, which can be performed from the ground state using two-colour resonance-enhanced multiphoton ionization (REMPI) [15, 35, 36]. For instance, photoionization via $n = 2$ requires a $\lambda = 243.0$ nm (UV) laser for the first transition and a $\lambda \leq 729.0$ nm (IR) laser to drive the excited state to the continuum. Positrons released from photoionized Ps can be accelerated by an electric field towards the target, and are there likely to annihilate.

(iii) Field ionization of high-n states [37]. Ps atoms excited to Rydberg levels $n \geq 17$ can be field ionized in an electric field $|\vec{F}| \approx 1.5$ kV cm^{-1} [14]. The two-photon excitation scheme used in Ref. [14] is similar to that described in (ii), except the IR wavelength is in the range of 730 to 770 nm. As with (ii), an appropriate electric field can be used to accelerate the released positrons towards the target.

The laser-Ps-interaction region is typically chosen to be very close (< 1 mm) to the Ps-formation region so that the maximum number of atoms can be addressed before the cloud disperses. Accordingly, processes (i) and (ii) normally occur during the prompt peak. In the case of (iii), the excitation and electric field regions do not necessarily overlap and, therefore, ionization may be delayed by the Rydberg Ps flight time.

A simulation has been made to study the overlap between a Ps source and a pulsed laser field [38]. Monte-Carlo techniques were used to simulate Ps distributions consistent with those created in experimental systems [e.g., 20]. Namely, a million positrons in a 4 mm wide 5 ns pulse are converted into Ps ($\epsilon = 0.3$). The Ps atoms are emitted from a plane surface (xy) with a cosine angular distribution [39], and with a speed distribution corresponding to $T = 600$ K. Shortly after ($t = 15$ ns), a 4 ns laser pulse tuned to the $1^3S \rightarrow 2^3P$ transition passes through the cloud along the x-direction, offset by a distance of 0.5 mm from the Ps-converter. The height ($\Delta y = 8$ mm) and width ($\Delta z = 3$ mm) of the flat profile of the laser field mimics that of a pulsed dye laser. The time-integrated laser intensity and spectral overlap are computed for each atom and those that surpass a given threshold are deemed to have been excited by the laser, as shown in Fig. 4.

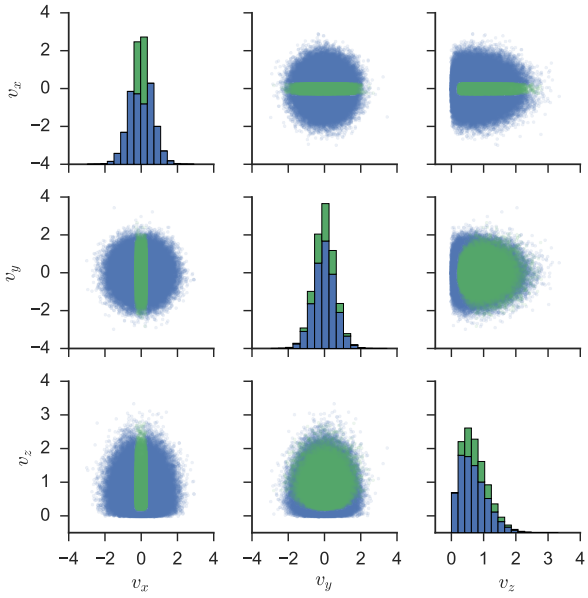

Figure 4. The velocity components (units of 10^5 m s^{-1}) of a simulated Ps distribution ($T = 600$ K). Atoms excited by a $\lambda = 243.0$ nm, $\Delta\nu = 100$ GHz, $\Delta t = 5$ ns laser pulse, which propagates parallel to the x-axis at $t = 15$ ns, are shown in green.

Doppler effects and the laser bandwidth leads to selection based on the x-component of the velocity distribution. To a lesser extent, the z and y components also restrict the range of atoms selected. This is due to the finite size of the laser profile: some of the Ps atoms pass through the interaction region before or after the laser pulse arrives, or miss it altogether. The simulation suggests that the laser is able to excite almost a quarter of the Ps atoms. However, if the

positron pulse is not radially compressed or not sufficiently bunched, or if the laser is positioned too far from the Ps-converter, the overlap can be very much reduced.

Monte-Carlo methods were also be used to generate an SSPALS spectrum for the simulated distribution. The Ps atoms were randomly assigned their lifetimes according to a mean value of 142 ns. The *"time of death"* was then found for each atom, as well as for the positrons that were not converted, and these times were collected into a histogram of 1 ns bins. The histogram was then convolved with the time-response of $PbWO_4$, producing an SSPALS lifetime spectrum that is consistent with Eq. 1. The spectrum was then re-calculated assuming that those Ps excited by the laser are ionized via REMPI and instantly annihilate. As shown in Fig. 5, this increases the number of annihilation events observed during the prompt peak, at the expense of those at later times.

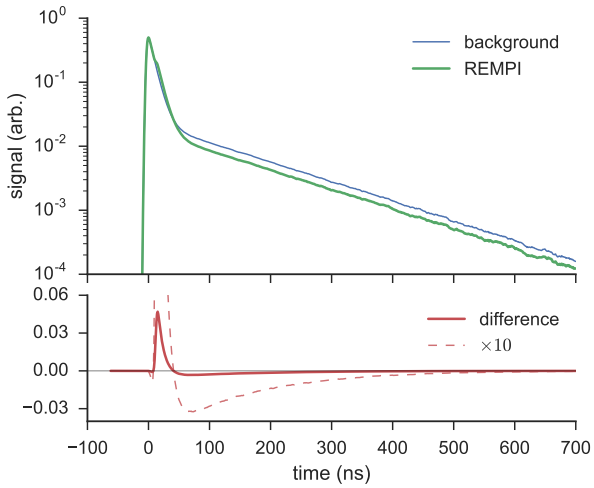

Figure 5. Monte-Carlo simulation of SSPALS spectra ($\epsilon = 0.3$, $\tau = 142$ ns, $\kappa = 9$ ns, and $\sigma = 2$ ns), including the effect of REMPI via $n = 2$. The UV laser ($\lambda = 243.0$ nm, $\Delta\nu = 100$ GHz) was triggered at $t = 15$ ns. The lower panel shows the background subtracted gamma-ray signal.

The difference between the background and REMPI simulated SSPALS spectra is a result of 23.7 % of the Ps atoms having been photoionized. As this fraction is known, the simulation also provides a way to evaluate the delayed fraction analysis techniques outlined in Sec. 2. Figure 6 shows the ionized fraction (lines) compared to values for S_γ (points) obtained from the simulated spectra for various laser wavelengths and delays, and for two different Ps distributions ($T = 600$ K and 1800 K). The delayed fraction was measured using $A = -10$ ns, $B = 35$ ns, and $C = 700$ ns; the value for $t = 0$ was found using a constant-fraction-discriminator (CFD) algorithm [40, 41] that triggers on the rising edge of the prompt peak.

Figure 6a illustrates how the temperature of the underlying Ps distribution can be inferred from the measured Doppler width of the Lyman-α transition [12, 13]. It also demonstrates that the S_γ parameter is a good estimate for the fractional change in the number of long-lived Ps. Magnetic quenching or field ionization of Rydberg states would produce a similar signal, which could equally be used for laser spectroscopy. (For magnetic quenching [e.g., 30] a smaller S_γ should be expected as not all of the 2^3P manifold can be magnetically mixed with the 2^1P level, whereas they can all be photoionized or excited to higher$-n$ states.)

The laser delay scan plotted in Fig. 6b indicates that S_γ does not always track the ionized fraction well; particularly for later laser trigger times, where $S_\gamma \approx 0$ despite the ionized fraction being significant. This is a consequence of the definition of the delayed fraction (Eq. 2) and

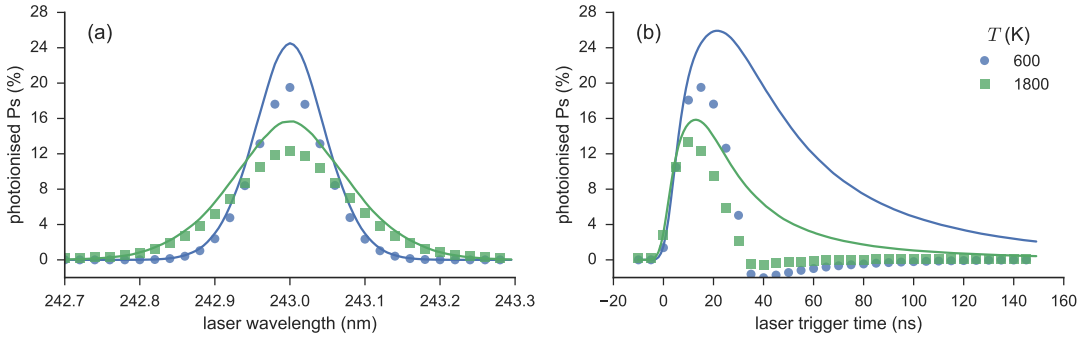

Figure 6. Monte-Carlo simulation of REMPI via $n = 2$. (a) For a range of UV laser wavelengths [t = 15 ns], (b) for different laser delays [λ = 243.0 nm], and for two different temperature distributions. The solid lines show the photoionized fraction; the points mark the S_γ values obtained by analysing the corresponding change in f_d, using $B = 35$ ns.

the choice of B. If a given Ps atom is photoionized after B then the net change to f_d will be zero, as in all likelihood it would have annihilated within the $B \to C$ time window anyway. The problem can be solved by extending B beyond the laser trigger time, or by choosing integration bounds that change according to the laser timing. If this type of measurement is performed with a sufficiently well-defined laser position then Ps time-of-flight spectra and longitudinal velocity information can be extracted [35].

3.3. Extending the lifetime of positronium

The 142 ns mean lifetime of ground-state o-Ps imposes a significant restriction on experiments. However, self-annihilation of Rydberg states ($n \gtrsim 10$) is almost negligible. The high-n states can be populated using pulsed lasers [14, 42–44], allowing for studies over timescales bounded by the fluorescence lifetime; for $n = 10 - 19$ this ranges over $3 - 26$ μs [45]. Long flight paths of more than a meter are therefore possible, even for Rydberg Ps atoms with fairly low kinetic energy. This allows for background-free detection using, for instance, a micro-channel plate (MCP) removed from the production environment [46, 47]. Nevertheless, SSPALS can also be used for experiments with Rydberg positronium [14, 43], and is relatively simple to implement.

The Monte-Carlo simulation was adapted such that, rather than photoionizing Ps, the laser increases the average lifetime to 2 μs. The simulated excitation scheme is a two-step transition via $n = 2$. I assume that the second step is 50 % likely for all atoms selected by the laser during the first step (as described in Sec. 3.2). The possibility of Ps colliding with the walls of a vacuum chamber was also included. The simulated chamber is an infinitely long tube, aligned to the z-axis, with an internal diameter of 40 mm. Histograms of the time and position of annihilation found for each of the simulated Ps atoms are shown in Fig. 7. Also shown are the various possible ways for a positron to expire, namely: direct annihilation (positrons/ p-Ps), o-Ps decay in vacuum, Rydberg Ps decay in vacuum, and Ps hitting the chamber.

The simulation indicates that the delayed annihilation events are dominated by o-Ps decay and collisions with the wall, rather than the decay of the excited states, even for fairly short-lived Rydberg levels (2 μs). It also shows that the vast majority of ground-state o-Ps will travel less than 50 mm before annihilating. Housing the Ps-converter in a fairly small vacuum chamber allows for the SSPALS detector to be positioned very near to the laser-interaction region. The 40 mm diameter chamber used in the simulation gives typical Ps flight times to the walls of a few hundred ns. Therefore, the walls are too far away for most ground-state Ps to reach but are well within the range of Rydberg Ps.

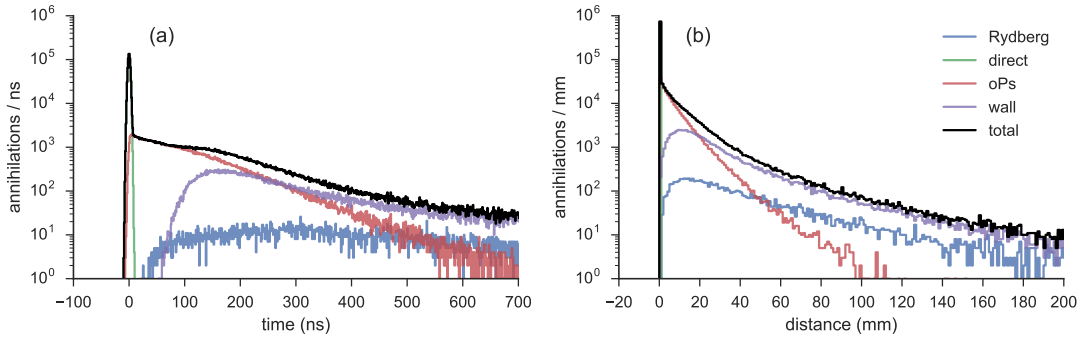

Figure 7. Histograms of (a) time and (b) z-position of a million annihilation events for Monte-Carlo simulated positrons converted to Ps ($T = 600$ K) and excited to Rydberg levels.

The time-binned annihilation events were convolved with the detector function to produce an SSPALS spectrum, which is plotted in Fig. 8. Also shown is a background (no laser) result, and the difference between them. In both cases, the inclusion of collisions with the chamber adds a broad lump to the spectra at $t \sim 200$ ns. The simulation suggests that when pulsed lasers are used to excite Ps atoms to long-lived Rydberg levels, the SSPALS spectrum will be affected by the disappearance of the early part of the 142 ns component, followed by the appearance of events at later times [20]. The extra delayed events distort the exponential tail and are typically evident even when the Rydberg levels have very long fluorescence lifetimes, as a consequence of the excited Ps atoms hitting the chamber walls. For $B = 35$ ns, the delayed fraction analysis gives $S_\gamma \approx 1.6$ %. This apparent insensitivity to Rydberg production can be remedied by setting B to 250 ns, which yields $S_\gamma = -39.5$ %. The value of B can be tuned to optimize the S_γ signal-to-noise ratio [18]. In practice, the optimal integration bounds will depend on the Ps velocity distribution, the surroundings, the detector location, the scintillation decay time, and background noise levels.

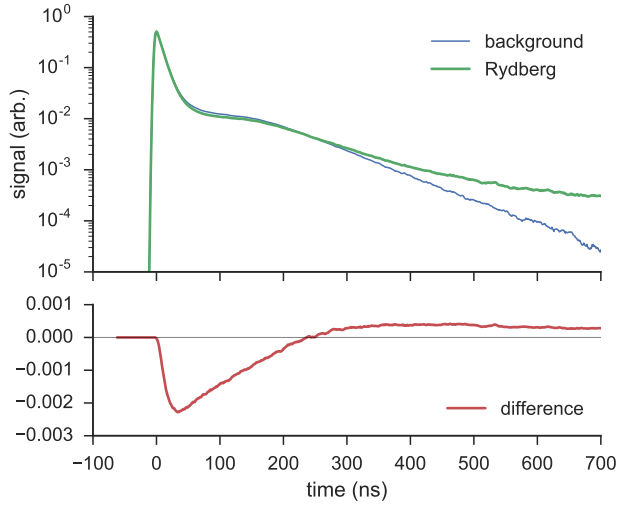

Figure 8. Monte-Carlo simulation of SSPALS spectra ($\epsilon = 0.3$, $\tau = 142$ ns, $\kappa = 9$ ns, and $\sigma = 2$ ns), including the effect of populating Rydberg levels via $n = 2$. The laser was triggered at $t = 15$ ns. The lower panel shows the background subtracted gamma-ray signal.

Here, the negative sign of S_γ is in contrast to the positive values found for the processes described in Sec. 3.2. Also, as B must be set to a later time, the delayed fraction is not representative of the number of o-Ps contributing to the spectra (see Sec. 2); nor should f_d be considered *the delayed fraction* in the previous sense. Although $S_\gamma \approx -39.5$ % is an indication of Ps being excited to long-lived Rydberg levels, its value is not a good measure of how many of the atoms are (~ 12 %). Moreover, the value of S_γ can vary significantly depending on the choice of B.

An example of an application of SSPALS to atomic physics experiments with positronium is given in Fig. 9 (from Ref. [14]). Ps atoms were formed by implanting 4 keV positrons into mesoporous silica. The emitted Ps distribution was then exposed to UV and IR laser pulses that had been tuned to drive $1S \rightarrow 2P \rightarrow nS/D$ transitions. A grid electrode placed 8 mm in front of the silica target set the electric field in the laser-interaction region to $|\vec{F}| \approx 0$. The IR laser was scanned over the wavelength range needed to populate $n = 9 - \infty$. And the corresponding SSPALS spectra were integrated to find f_d (using $A = -2$ ns, $B = 226$ ns, and $C = 597$ ns).

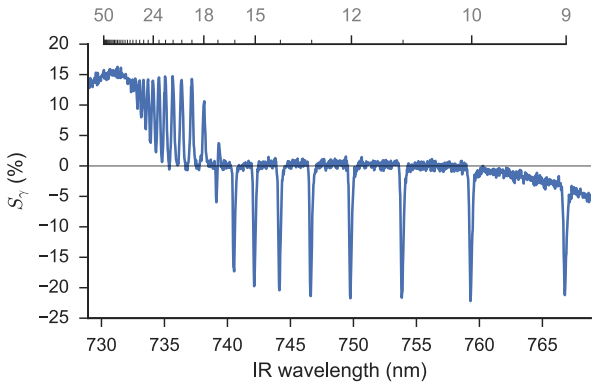

Figure 9. Spectrum of Ps excited to Rydberg levels via $n = 2$ in zero applied electric field. The top axis marks the expected location of each n-state. The integration bounds were $A = -2$ ns, $B = 226$ ns, and $C = 597$ ns. Data from Ref. [14].

Analysis of the SSPALS data resulted in sharp peaks in S_γ at the IR wavelengths expected to excite Ps from $n = 2$ to $n = 9 - 28$. For $n < 17$ the peaks are negative, indicating population of Rydberg levels that generally live longer than ground-state atoms. However, for $n > 17$ the peaks are positive, indicating average lifetimes that are shorter than those of the ground-state atoms. The authors attributed the latter to field ionization [37] of the $n > 17$ states as they passed through the grid (the electric field strength was estimated to be $|\vec{F}| \approx 1.5$ kV cm^{-1} directly between the mesh wires). This was verified by lowering the fields to allow $n = 18$ to pass, causing S_γ to flip from positive to negative. The split $n = 17$ line in Fig. 9 indicates excitation to states with either longer- or shorter-than-ground-state lifetimes, depending on which side of the Stark manifold the IR laser was tuned to. The large bandwidth of the UV laser (85 GHz) limited resolution of individual Rydberg levels to $n \lesssim 28$.

4. Concluding remarks

Single-shot positron annihilation lifetime spectroscopy (SSPALS) [16] is well suited to laser spectroscopy with positronium. This assertion is supported by a Monte-Carlo simulation that was used to examine the overlap between a time-bunched Ps distribution and a pulsed laser. In agreement with recent experiments [e.g., 12–15], the simulation indicates SSPALS can be used to observe laser induced processes that either reduce (Sec. 3.2) or extend (Sec. 3.3) the overall lifetime of Ps atoms.

Various assumptions and approximations were used to simplify the calculations, and numerous other effects were knowingly overlooked. For instance, Ps atoms can take several ns to escape from mesoporous silica [35, 48] and will have a reduced mean lifetime when inside the pore network [49]. The thermal speed and cosine angular distributions assumed for the Ps ensemble are unlikely to be very realistic, particularly for Ps emission from a mesoporous material. Positrons released from ionized Ps will not necessarily annihilate immediately, and could form new o-Ps atoms. The position of annihilation will determine the detector's solid-angle view of each event, thus lifetime spectra can be distorted by Ps dispersal. The fine-structure of the excited states and laser polarization can significantly affect transition rates, however, only a laser fluence threshold condition and each atom's Doppler shift were considered in determining if excitation events took place. In principle, these details (and many more [e.g., 50]) could be added to the simulation, nevertheless, the processes that were included are sufficient to explain the majority of features observed in experiments.

Using SSPALS for laser spectroscopy in the manner described in this work requires a background measurement of the delayed fraction. In the perfect world constructed in a simulation, this can be trivially derived from the lifetime spectra obtained when laser effects aren't included. In the less tractable world accessible to experimentalists, however, the background measurement warrants further consideration. The obvious choice is to measure lifetime spectra without the laser, although this could lead to non-resonant differences between the signal and background, e.g., due to laser-enhanced Ps emission [28]. Usually, the laser present but detuned from resonance provides a satisfactory background. But for two-photon transitions, such as the Rydberg spectroscopy measurements discussed in Sec. 3.3, there can be additional complications. For example, if the IR laser is detuned to prevent excitation to Rydberg levels but the UV laser still populates $n = 2$, then it's possible that the background spectrum will contain a magnetic quenching signal that's suppressed when the IR laser is on resonance. However, if the UV laser is also de-tuned then there will be no magnetic quenching in the background but could still be some in the signal measurement, particularly if the two lasers don't perfectly overlap. In general, these effects are hard to eradicate completely and may add features to background-subtracted spectra.

Another thing that should be considered when implementing SSPALS is the acquisition rate of lifetime spectra. In some cases, this may be determined by experimental requirements. For example, high-density Ps is needed to create di-positronium (Ps_2) [51, 52]. This will usually require many minutes of positron accumulation for every measured spectrum, imposing acquisition rates on the order of mHz. But if high densities are not needed, it can be statistically advantageous to run at a faster repetition rate (e.g., 1 Hz) and average measurements from many lifetime spectra [20].

My objective with this article was to employ a Monte-Carlo simulation to investigate SSPALS as a tool for atomic physics experiments with positronium. The power of SSPALS in this application is its simplicity and that it can be adapted to several different types of experiment. Delayed fraction analysis has proven a robust method for quantifying lifetime spectra, and it's well-suited to measuring various laser-induced distortions. However, more sophisticated analysis methods can extract more information [35], and could conceivably improve the signal-to-noise ratio of spectroscopic measurements. An improved understanding of how and why lifetime spectra are affected by the processes discussed in this work could lead to better analysis techniques, or could be exploited in designing new experiments.

Acknowledgments
I'm grateful to David Cassidy for many helpful discussions regarding this work. Funding was provided by the EPSRC (Grant No. EP/K028774/1). The Monte-Carlo simulations [38] were written using IPython [53].

References

[1] Ruark A E 1945 *Phys. Rev.* **68** 278

[2] Deutsch M 1951 *Phys. Rev.* **82**(3) 455–456

[3] Al-Ramadhan A H and Gidley D W 1994 *Phys. Rev. Lett.* **72**(11) 1632–1635

[4] Vallery R S, Zitzewitz P W and Gidley D W 2003 *Phys. Rev. Lett.* **90**(20) 203402

[5] Rich A 1981 *Rev. Mod. Phys.* **53** 127

[6] Knoll G F 2010 *Radiation detection and measurement* (New York, NY : Wiley) ISBN 9780470131480

[7] Siegel R W 1980 *Ann. Rev. Mat. Sci.* **10** 393–425

[8] Peng H G, Frieze W E, Vallery R S, Gidley D W, Moore D L and Carter R J 2005 *Appl. Phys. Lett.* **86** 121904

[9] Ley R 2002 *Appl. Surf. Sci.* **194** 301–306

[10] Chu S and Mills Jr A P 1982 *Phys. Rev. Lett.* **48**(19) 1333–1337

[11] Ziock K P, Dermer C D, Howell R H, Magnotta F and Jones K M 1990 *J. Phys. B At. Mol. Opt.* **23** 329

[12] Cassidy D B, Crivelli P, Hisakado T H, Liszkay L, Meligne V E, Pérez P, Tom H W K and Mills Jr A P 2010 *Phys. Rev. A* **81** 12715

[13] Deller A, Edwards D, Mortensen T, Isaac C A, van der Werf D P, Telle H H and Charlton M 2015 *J. Phys. B At. Mol. Opt. Phys.* **48** 175001

[14] Wall T E, Alonso A M, Cooper B S, Deller A, Hogan S D and Cassidy D B 2015 *Phys. Rev. Lett.* **114** 173001

[15] Aghion S, Amsler C, Ariga A, Ariga T, Bonomi G, Bräunig P, Bremer J, Brusa R S, Cabaret L, Caccia M, Caravita R, Castelli F, Cerchiari G, Chlouba K, Cialdi S, Comparat D, Consolati G, Demetrio A, Di Noto L, Doser M, Dudarev A, Ereditato A, Evans C, Ferragut R, Fesel J, Fontana A, Forslund O K, Gerber S, Giammarchi M, Gligorova A, Gninenko S, Guatieri F, Haider S, Holmestad H, Huse T, Jernelv I L, Jordan E, Kellerbauer A, Kimura M, Koettig T, Krasnicky D, Lagomarsino V, Lansonneur P, Lebrun P, Lehner S, Liberadzka J, Malbrunot C, Mariazzi S, Marx L, Matveev V, Mazzotta Z, Nebbia G, Nedelec P, Oberthaler M, Pacifico N, Pagano D, Penasa L, Petracek V, Pistillo C, Prelz F, Prevedelli M, Ravelli L, Resch L, Rienäcker B, Røhne O M, Rotondi A, Sacerdoti M, Sandaker H, Santoro R, Scampoli P, Smestad L, Sorrentino F, Spacek M, Storey J, Strojek I M, Testera G, Tietje I, Vamosi S, Widmann E, Yzombard P, Zmeskal J and Zurlo N (AEgIS Collaboration) 2016 *Phys. Rev. A* **94**(1) 012507

[16] Cassidy D B, Deng S H M, Tanaka H K M and Mills Jr A P 2006 *Appl. Phys. Lett.* **88** 137–140

[17] Cassidy D B and Mills Jr A P 2007 *Nucl. Instrum. Meth. A* **580** 1338–1343

[18] Alonso A, Cooper B, Deller A and Cassidy D 2016 *Nucl. Instrum. Meth. A* **828** 163 – 169

[19] Cassidy D B, Deng S H M, Greaves R G, Maruo T, Nishiyama N, Snyder J B, Tanaka H K M and Mills Jr A P 2005 *Phys. Rev. Lett.* **95** 195006

[20] Cooper B S, Alonso A M, Deller A, Wall T E and Cassidy D B 2015 *Rev. Sci. Instrum.* **86** 103101

[21] Liszkay L, Corbel C, Perez P, Desgardin P, Barthe M F F, Ohdaira T, Suzuki R, Crivelli P, Gendotti U, Rubbia a, Etienne M and Walcarius a 2008 *Appl. Phys. Lett.* **92** 137–140

[22] Mariazzi S, Bettotti P and Brusa R S 2010 *Phys. Rev. Lett.* **104**(24) 243401

[23] Crivelli P, Gendotti U, Rubbia A, Liszkay L, Perez P and Corbel C 2010 *Phys. Rev. A* **81** 52703

[24] Mills Jr A P and Pfeiffer L 1985 *Phys. Rev. B* **32** 53–57

[25] Cooper B S, Alonso A M, Deller A, Liszkay L and Cassidy D B 2016 *Phys. Rev. B* **93**(12) 125305

[26] Cialdi S, Boscolo I, Castelli F, Villa F, Ferrari G and Giammarchi M G 2011 *Nucl. Instrum. Meth. B* **269** 1527

[27] Fee M S, Mills Jr A P, Chu S, Shaw E D, Danzmann K, Chichester R J and Zuckerman D M 1993 *Phys. Rev. Lett.* **70** 1397–1400

[28] Cassidy D B, Hisakado T H, Tom H W K and Mills Jr A P 2011 *Phys. Rev. B* **84**(19) 195312

[29] Alonso A M, Cooper B S, Deller A, Hogan S D and Cassidy D B 2015 *Phys. Rev. Lett.* **115**(18) 183401

[30] Alonso A M, Cooper B S, Deller A, Hogan S D and Cassidy D B 2016 *Phys. Rev. A* **93**(1) 012506

[31] Curry S M 1973 *Phys. Rev. A* **7** 447–450

[32] Cassidy D B, Hisakado T H, Tom H W K and Mills Jr A P 2011 *Phys. Rev. Lett.* **106** 173401

[33] Alekseev A I 1958 *Sov. Phys. JETP* **34** 1312

[34] Alekseev A I 1958 *Sov. Phys. JETP* **34** 826

[35] Deller A, Cooper B S, Wall T E and Cassidy D B 2015 *New J. Phys.* **17** 043059

[36] Cassidy D B, Bromley M W J, Cota L C, Hisakado T H, Tom H W K and Mills A P 2011 *Phys. Rev. Lett.* **106**(2) 023401

[37] Gallagher T F 2005 *Rydberg atoms* Cambridge Monographs on Atomic, Molecular and Chemical Physics (Cambridge University Press) ISBN 9780521021661

[38] Deller A 2016 mc_sspals URL https://doi.org/10.5281/zenodo.154045

[39] Greenwood J 2002 *Vacuum* **67** 217 – 222 ISSN 0042-207X

[40] Gedcke D A and McDonald W J 1967 *Nucl. Instrum. Meth.* **55** 377–380

[41] Deller A 2016 python tools for SSPALS URL http://dx.doi.org/10.5281/zenodo.61489

[42] Ziock K P, Howell R H, Magnotta F, Failor R A and Jones K M 1990 *Phys. Rev. Lett.* **64** 2366–2369

[43] Cassidy D B, Hisakado T H, Tom H W K and Mills Jr A P 2012 *Phys. Rev. Lett.* **108** 043401

[44] Jones A C L, Hisakado T H, Goldman H J, Tom H W K, Mills Jr A P and Cassidy D B 2014 *Phys. Rev. A* **90**(1) 012503

[45] Deller A, Alonso A M, Cooper B S, Hogan S D and Cassidy D B 2016 *Phys. Rev. A* **93**(6) 062513

[46] Jones A C L, Goldman H J, Zhai Q, Feng P, Tom H W K and Mills Jr A P 2015 *Phys. Rev. Lett.* **114**(15) 153201

[47] Jones A C L, Hisakado T H, Goldman H J, Tom H W K and Mills Jr A P 2016 *J. Phys. B At. Mol. Opt.* **49** 064006

[48] Cassidy D B, Hisakado T H, Meligne V E, Tom H W K and Mills A P 2010 *Phys. Rev. A* **82**(5) 052511

[49] Gidley D W, Frieze W E, Dull T L, Yee A F, Ryan E T and Ho H M 1999 *Phys. Rev. B* **60**(8) R5157–R5160

[50] Hughes V W, Marder S and Wu C S 1955 *Phys. Rev.* **98**(6) 1840–1848

[51] Cassidy D B and Mills Jr A P 2007 *Nature* **449** 195–197

[52] Cassidy D B, Hisakado T H, Tom H W K and Mills Jr A P 2012 *Phys. Rev. Lett.* **108**(13) 133402

[53] Pérez F and Granger B E 2007 *Comput. Sci. Eng.* **9** 21–29 ISSN 1521-9615